Exploration on 1n halo nucleus ^{19}C from D-RHFB structure to reaction observables

Jia-Lin An[a,c], Qi Lu[a], Wen Hui Long[b,d,*], Shi-Sheng Zhang[a,*]

[a] *School of Physics, Beihang University, Beijing, 100191, China*
[b] *Frontier Science Center for Rare isotope, Lanzhou University, Lanzhou, 730000, China*
[c] *Baoding Hospital of Beijing Children's Hospital, Baoding, Hebei, 071000, China*
[d] *Joint Department for Nuclear Physics, Lanzhou University and Institute of Modern Physics, CAS, Lanzhou, 730000, China*

Abstract

We utilize the axially deformed relativistic Hartree-Fock-Bogoliubov (D-RHFB) model to describe the structure of neutron-rich carbon isotopes, taking into account the continuum, pairing correlations, tensor force and their interplay. In this scheme, one- and two-neutron separation energies of neutron-rich carbon isotopes agree well with measured data, as well as the spin and parity $J^\pi = 1/2^+$ for the ground state of ^{19}C, which is a long-standing problem for theoretical structure models. With the structure input extracted from the microscopic D-RHFB model, the reaction observables are well described the Glauber model. In particular, this unified approach accurately reproduces the inclusive longitudinal momentum distributions of the breakup reaction ^{19}C + ^{12}C at 240 MeV/nucleon, which rule out the possibility of the ground state of ^{19}C being $J^\pi = 3/2^+$. Moreover, the continuum plays a crucial role in the formation of the halo, which is further confirmed by the reaction cross sections and longitudinal momentum distributions. However, the tensor force components carried by the π-coupling are not as significant as anticipated. Consequently, the D-RHFB + Glauber approach turns out to be a promising tool to search for halo candidates from the structure to the reaction.

Keywords: ^{19}C halo, continuum, tensor effect, Glauber model, reaction cross section, inclusive longitudinal momentum distribution

1. Introduction

High-energy nucleon removal reactions have emerged as a valuable tool to investigate the structure of neutron-rich nuclei far from the valley of stability. These exotic nuclei close to the neutron drip line exhibit a range of novel properties, including halo phenomena, inversion of the island, and the emergence of new magic numbers [1].

The study of neutron-rich carbon isotopes has attracted significant interest due to the co-existence of both shell structure and halo distributions. For instance, the substantial proton subshell gap of $Z = 6$ was evidenced through the measurement of the lifetime for the excited state 2^+ in even-even neutron-rich carbon isotopes [2–6]. Furthermore, the potential neutron subshell closure of $N = 16$ was identified in the pursuit of the two-neutron halo nucleus ^{22}C [7].

For the odd-A nucleus ^{19}C, the one-neutron (1n) halo structure is widely accepted with a small neutron separation energy ($S_n = 0.572$ MeV). However, the spin and parity of its ground state (g.s.) are difficult to be confirmed through measurements over the past three decades. Moreover, the formation of a halo nucleus remains a subject of debate, with a lack of a unified description from microscopic structure to reaction observables. This is mainly due to the ambiguity and complexities of the nuclear structure. Consequently, a comprehensive study on ^{19}C will be beneficial to gain a deeper understanding of the crucial factors for new 1n halo nuclei.

Experimentally, the momentum distributions of the residues after the break-up reaction of a halo nucleus bombarding a carbon/berilium target have been regarded as a crucial probe for spatially extended wave functions of the valence neutron [8–10]. This reveals the orbital angular momentum of the removed valence nucleon(s) close to the Fermi surface. Narrow longitudinal momentum distributions of the ^{18}C fragments have been observed following the breakup reaction of the ^{19}C on a carbon target at approximately 910 [8] and 240 [10] MeV/nucleon, respectively. Moreover, the reaction cross section of ^{19}C + ^{12}C at 960 MeV/nucleon has been previously measured [11], while the most recent measurement at 307 MeV/nucleon yielded a larger uncertainty [7]. In contrast to the aforementioned experiments, a comprehensive measurement of Coulomb dissociation of ^{19}C at 67 MeV/nucleon was conducted [12], resulting in a large $E1$ cross section with a peak $E_{rel} = 300$ keV. Recently, the proton radii of the isotopes $^{12-19}$C have been derived from accurate charge-changing cross section measurements at 900 MeV/nucleon with a carbon target [13]. In a related study, Maddalena *et al.* detected the reaction cross sections and longitudinal momentum distributions of the 1n knockout reactions when changing the target from ^{12}C to ^{9}Be, at about 60 MeV/nucleon [9]. The results of the aforementioned experiments indicate that the presence of a 1n halo in ^{19}C is widely accepted. However, the ambiguity regarding the spin and parity ($J^\pi = 1/2^+$ or $3/2^+$) of the g.s. for ^{19}C still exists, despite the

*Corresponding Author
Email addresses: longwh@lzu.edu.cn (Wen Hui Long), zss76@buaa.edu.cn (Shi-Sheng Zhang)

aforementioned measurements and theoretical analysis [8–13].

In parallel with the experimental progress, numerous theoretical efforts have been made during the last three decades. Based on a shell model calculation with Warburton-Brown interactions, the g.s. with $J^\pi = 5/2^+$ was proposed [14]. Ridikas *et al.* calculated the longitudinal momentum distributions based on a neutron-plus-core coupling model, assuming two possibilities for the g.s. in ^{19}C with a deformed Woods-Saxon potential: $J^\pi = 1/2^+$ and $J^\pi = 3/2^+$ [15]. A comprehensive analysis of experimental data at 88 and 910 MeV/nucleon was carried out by Kanungo *et al.* using the Glauber model to study three possibilities, namely $J^\pi = 1/2^+, 3/2^+$ and $5/2^+$ for the g.s. configurations in ^{19}C, with different constraints on the $1n$ separation energies. The authors noted that a significant alteration of the core of ^{19}C from the bare ^{18}C nucleus may occur [16]. Definitely, the potential exerts a pivotal influence on the spin and parity of the g.s. and the separation energy of ^{19}C. For the power of prediction, a microscopic potential obtained by a self-consistent calculation is highly desirable.

In a recent study, Sun and Zhou *et al.* employed the DRHBc theory to investigate the $^{14-22}$C isotopes, resulting in the identification of the $1/2^+$ orbital for ^{19}C, which corresponds to the second minimum of the binding energy [17]. The incorporation of these DRHBc calculations [18] with the Glauber model has led to the successful confirmation of ^{15}C as a $1n$ halo at an incident energy of 80 MeV/nucleon. Conversely, the evidence for ^{19}C as a $1n$ halo nucleus appears to be weak, as indicated by the momentum distributions of the break-up reaction [19]. This aspect is further considered in this Letter. In the context of an effective field theory, Acharya *et al.* concluded that a dominant s-wave configuration of the valence neutron is responsible for a halo in ^{19}C, based on an overall normalized momentum distribution with a fitted peak [20]. Kanungo *et al.* then performed a coupled-cluster calculation to support ^{19}C as a prominent halo deduced from the extremely large radius [13]. Guo *et al.* employed a complex momentum representation method to investigate the bound and resonant states of ^{19}C in a deformed Woods-Saxon shape potential [21, 22]. They proposed that ^{19}C has a prolate halo with a dominant s-wave configuration. In the context of the CD-Bonn Gamow shell model, Xu *et al.* declared that the inclusion of the continuum coupling in their calculations is crucial for the accurate description of neutron-rich carbon isotopes. This approach has been demonstrated to reproduce the experimental g.s. of ^{19}C with $J^\pi = 1/2^+$ [23], thereby becoming a benchmark work for the Gamow shell model on this topic.

In addition to the DRHBc theory, the relativistic Hartree-Fock (RHF) theory and the extended relativistic Hartree-Fock-Bogoliubov (RHFB) theory [24–26] offer alternative solutions to study the isotope ^{19}C, incorporating the Fock terms. Over the past two decades, the RHF and RHFB theories have been sucessful in elucidating a multitude of nuclear phenomena, including the pseudo-spin symmetry [27–29], the emergence of new magicity [30–33], the formation of halo or bubble-like structures [34–38], and spin-isospin excitation [39–43]. The incorporation of the Fock terms within the RHF framework enables the consideration of the significant nuclear tensor force in a natural manner [44–48], which is crucial for the reliable description of exotic nuclei. In particular, the $1n$ halo structures in both ^{17}C and ^{19}C have been indicated by the RHFB calculations under the assumption of spherical symmetry [35]. Presently, both the RHF and RHFB theories have been extended and generalized to the axially deformed RHF and RHFB models, i.e., the D-RHF and D-RHFB models [49, 50], which provide a unified treatment of significant spin-orbit coupling, tensor force, nuclear deformation, pairing correlations, and the continuum effects for a wide range of exotic nuclei.

Regarding the importance of the continuum and deformation, we are motivated to study the microscopic structure and reaction observables of ^{19}C by combining the recently developed D-RHFB model and the Glauber model. In this Letter, we focus on the D-RHFB calculations of neutron-rich carbon isotopes, and aim at understanding the contributions from the continuum, pairing correlations, tensor force and their interplay in the formation of the deformed halo in ^{19}C. Furthermore, we investigate the impact of the continuum and the tensor force on the reaction observables resulting from the breakup reaction ^{19}C + ^{12}C, and distinguish the possibilities of different J^π (for the g.s.) in ^{19}C from the reaction observables. In such a unified way, we assess the validity and necessity of this new combination.

2. Numerical details

In order to obtain a reliable description of the carbon isotopes, a series of systematic calculations were performed by using a number of popular effective Lagrangians within the D-RHFB framework [50]. These included the RMF Lagrangian DD-ME2 [51], the RHF Lagrangians PKOi ($i = 1, 2, 3$) [24, 44] and PKA1 [25]. It has been demonstrated that the RHF Lagrangian PKO3, which incorporates the π-pseudo-vector (π-PV) coupling, provides the best description of the bulk properties of the neutron-rich carbon isotopes from ^{14}C to ^{22}C, encompassing the binding energies, separation energies, and matter radii. Unless otherwise specified, the subsequent calculations are conducted with PKO3.

In the D-RHFB calculations, the Bogoliubov quasi-particle (q.p.) and canonical single-particle (s.p.) wave functions have been expanded on the spherical Dirac Woods-Saxon (DWS) basis. This basis has the advantage of properly describing the asymptotic behavior of the s.p. wave functions for unstable nuclei [52]. The space truncation of the DWS basis has been carefully verified to guarantee the accuracy in practice. For carbon isotopes, the maximum values of the angular momentum projection m were chosen to be $9/2$ and $11/2$ for even- and odd-parity states, respectively. From these values, the maximum values of $|\kappa|$ in the spherical DWS basis were determined to be 9 and 10, respectively. Moreover, the spherical box size of the DWS basis was determined to be 24 fm with a mesh step size of 0.1 fm. The DWS basis states with positive (negative) energies, $E < E_+^C + M$ ($E > E_-^C - M$), were considered for the expansion of the q.p. orbits, where $E_+^C = 400$ MeV, $E_-^C = -100$ MeV and M is nucleon mass. A detailed explanation of the space truncation can be found Ref. [50].

For unstable open-shell nuclei, the pairing correlations play an important role, especially in the context of understanding the weak binding mechanism therein. In this work, we adopt the pairing force as the finite-range Gogny force D1S [53], which provides a natural energy cutoff in the pairing channels due to its finite-range nature.Since the pairing force was developed within a non-relativistic Gogny Hartree-Fock-Bogoliubov model, here the pairing force D1S is slightly adjusted by multiplying it with a strength factor in order to reproduce the observables [54, 55], such as the odd-even mass staggering along the isotopic chain of carbon [56]. In addition, the blocking effects for the odd carbon isotopes were considered. Specifically, the first q.p. state in a given m-block was blocked, and the one with the lowest energy of the nuclear system was regarded as the ground state.

Subsequently, the angle-averaged densities of the nuclear core and the wave function of the valence neutron provided by the D-RHFB model [57, 58] are used to obtain the reaction observables of ^{19}C on a carbon target, via the reaction Glauber model. For axially deformed nuclei, the angle-averaged densities correspond to the zeroth-order terms of the Legendre series of the density expansion, as described by Eq. (38b) in Ref. [49]. Details on the Glauber model are available in Refs. [59–61] and therein.

3. Results and discussions

Figure 1 shows the one-neutron (S_n) and two-neutron (S_{2n}) separation energies (in MeV) for carbon isotopes given by the D-RHFB calculations with PKO3, in comparison to the experimental data [56]. It is clearly seen that both values of S_n and S_{2n} for carbon isotopes are well reproduced. Moreover, the ground state configurations J^π of the odd isotopes ^{15,17,19}C are also correctly obtained, namely $J^\pi = 1/2^+$ for ^{15}C and ^{19}C [12], and $3/2^+$ for ^{17}C [62]. Indeed, it is challenging to identify a unified description of the ground state configurations for the odd carbon isotopes within relativistic energy density functional models. Motivated by the fact that the D-RHFB model with PKO3 provides a reliable description for the carbon isotopes, we further analyze the neutron halo structure of ^{19}C.

Figure 2 (a) depicts the contour map of proton (P) and neutron (N) densities (fm^{-3}) for ^{19}C, with the neutron $1/2^+$ state blocked. The neutron distribution is considerably more extensive than that of the protons, extending largely along both the x- and z-axes (the symmetric one). This is a typical feature of the halo phenomenon. Figure 2 (b) presents the distributions of the odd valence neutron and the neutrons populating the continuum. For the valence neutron, which blocks the first q.p. $1/2^+$ orbit, the distribution was calculated directly by using the q.p. wave function. The continuum distributions are obtained by subtracting the bound neutron contributions from the total one, using the canonical s.p. wave functions. From Fig. 2 (a), it can be observed that the dispersion of the neutron distribution is almost entirely attributable to the valence neutron, which supports a $1n$ halo structure for ^{19}C. As predicted for ^{44}Mg [63], there is also a clear shape decoupling between the $1n$ halo and

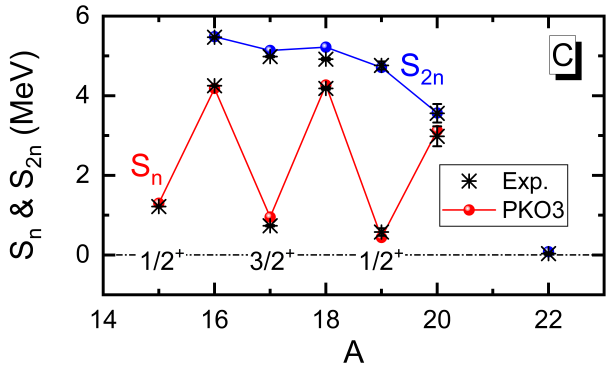

Figure 1: (Color Online) One- and two-neutron separation energies S_n and S_{2n} (MeV) for carbon isotopes. The sphere symbols (red/blue) represent the results (S_n/S_{2n}) given by the D-RHFB calculations with PKO3 [44], and the experimental (Exp.) data are taken from Ref. [56] for comparison.

the core of ^{19}C, which exhibit prolate and oblate shapes, respectively. On the other hand, as illustrated in the right side of Fig. 2 (b), the continuum plays a pivotal role in the formation of the halo nucleus.

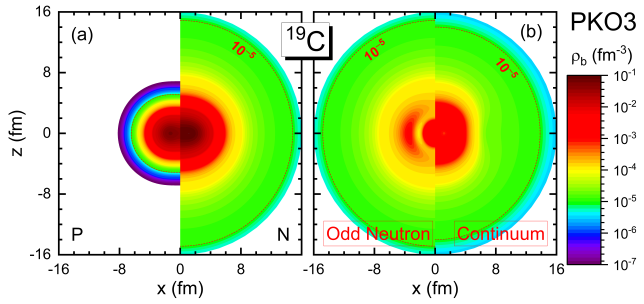

Figure 2: (Color Online) Panels (a) and (b) show the contour maps of neutron and proton densities (fm^{-3}) of ^{19}C, and the contributions from the odd neutron and continuum states, respectively. The results are given by the D-RHFB calculations with PKO3 for the case $J^\pi = 1/2^+$.

In order to provide a comprehensive understanding of the $1n$ halo, the proton and neutron canonical s.p. spectra of ^{19}C with $J^\pi = 1/2^+$ are presented in Figs. 3 (a) and (b), respectively. The lengths of the thick lines represent the occupation probabilities of the orbits. It is evident from the proton spectrum [plot (a)] that there is a shell at $Z = 6$, which results in the absence of pairing effects in the proton channel. This notable shell closure is consistent with the experimental evidence presented in Ref. [64]. In contrast to the simple proton spectrum, the neutron canonical s.p. spectrum in Fig. 3 (b) exhibits a typical weak binding feature. As illustrated in Fig. 3 (b), a substantial number of neutrons occupy the continuum (above the dash-dotted line), particularly the canonical $1/2^+_3$ orbit. It is noteworthy that the valence neutron blocking the first q.p. $1/2^+$ state is mapped into several canonical s.p. states (mainly $1/2^+_2$ and $1/2^+_3$), resulting in notable contributions to the continuum. Indeed, the D-RHFB calculations of blocking the $3/2^+$ state for ^{19}C yield similar order of neutron orbits. However, the valence neutron is almost fully mapped into the canonical $3/2^+_1$ orbits, which prevent populating from the continuum via the pairing correla-

tions. In contrast, for the $1/2^+$ case shown in Fig. 3 (b), the neutrons populating the canonical $3/2^+_1$ orbit become easier to be scattered into the continuum via the pairing correlations.

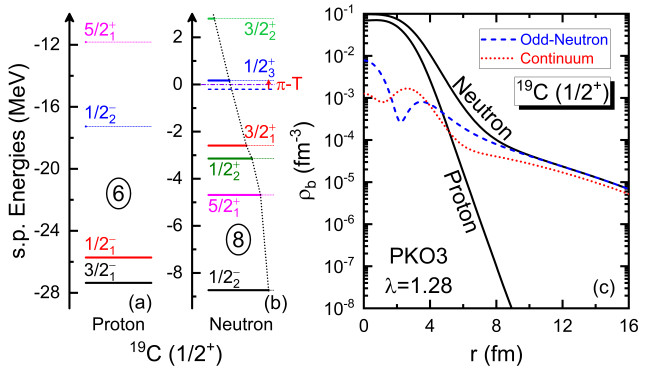

Figure 3: (Color online) Panels (a) and (b) show the neutron and proton canonical s.p. spectra of ^{19}C, respectively, and panel (c) presents the angle-averaged densities (fm^{-3}), including the neutron and proton ones, and the contributions from the odd neutron (blue dashed line) and the $1/2^+$ continuum states (red dotted line). The results are given by the D-RHFB calculations with PKO3 for the case $J^\pi = 1/2^+$, and the neutron orbit $1/2^+_3$ given by the calculation with deactivated π-T coupling (dashed line) is shown in panel (b) for comparison.

As a supplement, we would like to disclose that the canonical $1/2^+_3$ orbit contains approximately 48% $1d_{5/2}$ component, in accordance with the prolate continuum distribution observed in the right side of Fig. 2 (b). It is therefore not unexpected to observe the prolate orbit $1/2^+_3$ in the continuum, given that the entire nucleus ^{19}C is oblately deformed. Moreover, the tensor force is likely to play a role. As displayed in Fig. 3 (b), when excluding the tensor force component (π-T) carried by the π-PV coupling, the $1/2^+_3$ continuum orbit becomes weakly bound (thick dashed line). This can be explained by the considerable $1d_{5/2}$ proportion in the $1/2^+_3$ orbit, which presents repulsive tensor coupling with the core of ^{19}C, as deduced from the nature of the tensor force [49]. From this point of view, it is evident that the π-T coupling in PKO3 can notably enhance the continuum contributions. However, it should be noted that the halo extension is not significantly influenced. This can be demonstrated by the observation that the halo orbit $1/2_3$ is relatively weakly bound when the π-T coupling is deactivated.

To deeply understand the halo phenomenon in ^{19}C, Fig. 3 (c) depicts the angle-averaged densities (fm^{-3}) of neutron and proton (solid lines), the odd valence neutron (dashed line), and the $1/2^+$ continuum states (dotted line). It should be noted that the $1/2^+$ continuum originates mainly but not fully from the odd neutron. The results in Fig. 3 (c) are consistent with the dispersion of neutron density almost fully due to the odd neutron, with the $1/2^+$ continuum states presenting a substantial even dominant contribution to the halo of ^{19}C, as illustrated in Fig. 2 (b). The density distributions depicted in Fig. 3 (c), in conjunction with those of ^{18}C extracted from the D-RHFB calculations, were employed as input to compute the cross section and inclusive longitudinal momentum distributions, and search for the evidences of halo structure from the reaction observables.

As previously stated, the D-RHFB calculations with PKO3 reproduce the ground state $J^\pi = 1/2^+$ for ^{19}C, which is deeper

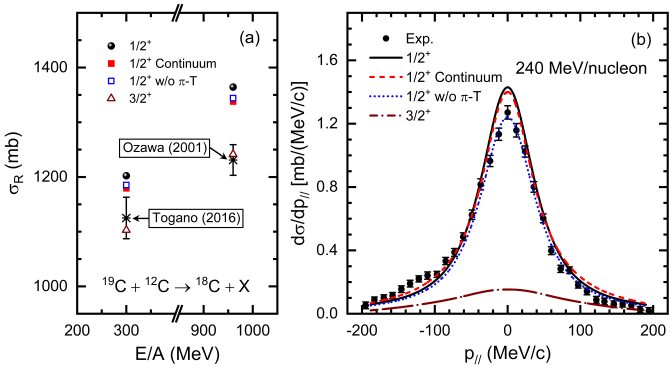

Figure 4: (Color online) Panels (a) and (b) show the reaction cross sections σ_R (mb) of ^{19}C on a carbon target at 300 (960) MeV/nucleon and the inclusive longitudinal momentum distribution $d\sigma/dp_{//}$ [mb/(MeV/c)] for breakup reaction ^{19}C + ^{12}C at 240 MeV/nucleon, respectively, in comparison to the experimental data. The results are calculated by the Glauber model with inputs from the D-RHFB theory, and the experimental data of σ_R (black stars) and $d\sigma/dp_{//}$ are taken from Refs. [7, 11] and [10], respectively. See the text for details.

bound than the $J^\pi = 3/2^+$ case by approximately 0.13 MeV. Therefore, we will examine the reaction observables of ^{19}C on a carbon target for both cases of $J^\pi = 1/2^+$ and $J^\pi = 3/2^+$. The Glauber model, as expressed in Eq. (1) of Ref. [61], was used to calculate the reaction cross sections (RCSs) σ_R of ^{19}C + ^{12}C at 300 (960) MeV/nucleon. The angle-averaged densities of the core and the odd neutron, which were extracted from the D-RHFB calculations, were utilized as inputs for the Glauber model. In this study, we considered different odd neutron densities provided by the D-RHFB model as inputs to gain a comprehensive understanding of the formation of a single-neutron halo in ^{19}C. These include the density of the odd neutron blocking the $1/2^+$ state ($J^\pi = 1/2^+$) and the $1/2^+$ continuum contributions therein, and the density of the odd neutron blocking the $3/2^+$ state ($J^\pi = 3/2^+$). In order to show the impact of the tensor force, the outcomes of the $J^\pi = 1/2^+$ calculation with deactivated π-T coupling in PKO3 are presented as well. The results are ploted in Fig. 4 (a), in comparison to the available data (black stars) [7, 11].

As displayed in Fig. 4 (a), the Glauber calculation with the $1/2^+$ odd neutron density (sphere symbols) yields larger σ_R values than the experimental data. The results of blocking the $3/2^+$ state (open up-triangles) appear within the experimental uncertainty. It is necessary to emphasize that the input densities employed in current Glauber calculations are angle-averaged, which smooth the deformation effects. Based on our experience with neon isotopes [65], we anticipate that all the calculated σ_R values will be reduced once the deformation effect is fully considered. In the case of $J^\pi = 1/2^+$, as compared to the full $1/2^+$ results (sphere symbols) in Fig. 4 (a), it is evident that the $1/2^+$ continuum (filled squares) plays a pivotal role in the determination of the cross section σ_R. This is in contrast to the situation (open squares) that when the π-T coupling in PKO3 is switched off, the cross sections are only slightly changed from the full PKO3 results (sphere symbols). These results are consistent with those in Figs. 2 and 3. As illustrated in Fig. 2, the halo formation of ^{19}C is largely due to the continuum, which

can be enhanced by the π-T coupling. This is demonstrated in Fig. 3 (b). When the π-T coupling is deactivated, the $1/2^+_3$ continuum orbit becomes rather weakly bound. It results in a reduction of the continuum contributions, yet the extension of the odd neutron distribution, which is responsible for the halo in ^{19}C, remains largely unaffected.

Besides the cross section σ_R, the longitudinal momentum distributions $d\sigma/dp_{//}$ for ^{18}C residues after the $1n$ removal reaction of ^{19}C at 240 MeV/nucleon bombarding a carbon target are calculated, using Eq. (5) in Ref. [61], and further folded by a Lorentzian function with an experimental resolution 23 MeV/c used in Ref. [10]. The results are presented in Fig. 4 (b), in comparison with the measured data [10]. It is evident that the results of the full $1/2^+$ odd neutron density (solid line) show a narrow peak shape for the momentum distributions of ^{18}C residues, which agree with the data. Moreover, the calculated full width at half maximum (FWHM) is approximately 86 MeV/c for ^{18}C residues, which is in a good agreement with the experimental value of 83(12) MeV/c [66]. This is in contrast to the value of 56 MeV/c in Ref. [10], folded by a Gaussian function with the same experimental resolution. However, the longitudinal momentum distributions for the case of blocking the $3/2^+$ state (long-dash dotted line) are rather flat, which reflects a compact structure in the coordinate space. In this way, the possibility of the g.s. with $J^\pi = 3/2^+$ has been ruled out, and the g.s. configuration $J^\pi = 1/2^+$ has been confirmed as strong evidence to form an $1n$ halo in ^{19}C.

Quantitatively, Table 1 lists the main spherical DWS basis components of the odd neutron blocking the first q.p. $1/2^+$ and $3/2^+$ orbits, respectively. In accordance with the results in Fig. 4, the $1/2^+$ contributions encompass the valence odd neutron ($1/2^{+a}$) and the $1/2^+$ continuum ($1/2^{+b}$) given by the D-RHFB calculations with PKO3, and the valence odd neutron ($1/2^{+c}$) resulting from the calculations with the π-T coupling deactivated. It is evident that the odd neutron blocking the $1/2^+$ state is dominated by the s-components, with the proportions of $2s_{1/2}$ and $3s_{1/2}$ components reading as 56.96% and 30.90%, respectively. These results are consistent with the longitudinal momentum distributions of ^{18}C residues with $J^\pi = 1/2^+$ in Fig. 4 (b). Such narrow momentum distributions are caused by substantial s-wave components, which are in accordance with the dilute space distributions given by the D-RHFB calculations, as shown in Figs. 2 (b) and 3 (c).

For the halo formation in ^{19}C, the significance of the continuum is clearly demonstrated by the results in Figs. 2 (b), 3 (c) and 4, from the structure to the reaction. In the following, we will further deepen our understanding on the $1n$ halo of ^{19}C, by focusing on the $1/2^+$ continuum contributions. As listed in Table 1, the $1/2^+$ continuum ($1/2^{+b}$) is dominated by the $3s$ and $1d$ components, which explain well the dispersion and prolate shape of the halo, respectively. It should be noted that the odd neutron fractions ($1/2^{+a}$) are extracted from the expansion of the blocked q.p. $1/2^+$ orbit, while the fractions the $1/2^+$ continuum are deduced from the expansions of the canonical $1/2^+$ continuum orbits upon the spherical DWS basis. As mentioned in discussing Fig. 3 (b), the odd neutron is primarily mapped into the canonical $1/2^+_2$ and $1/2^+_3$ orbits. From Table 1, it is thus

Table 1
Proportions (%) of the main spherical DWS basis components of the odd neutron for the configurations $J^\pi = 1/2^+$ and $3/2^+$, with the cases $1/2^{+a,b}$ for the odd neutron and the $1/2^+$ continuum states given by the full PKO3 calculations, respectively, and the case $1/2^{+c}$ for the odd neutron given by the calculations with deactivated π-T coupling in PKO3.

Cases	Main spherical DWS components				
	$2s_{1/2}$	$3s_{1/2}$	$4s_{1/2}$	$1d_{3/2}$	$1d_{5/2}$
$1/2^{+a}$	56.96%	30.90%	3.59%	2.57%	5.98%
$1/2^{+b}$	4.59%	34.13%	5.18%	11.31%	43.09%
$1/2^{+c}$	62.40%	25.18%	3.60%	1.99%	6.83%
$3/2^+$	–	–	–	23.84%	72.28%

deduced that the substantial $3s$ component in the $1/2^+$ continuum is predominantly attributed to the odd neutron, whereas the $1d$ ones originate mainly from paired neutrons. From this point of view, the formation and stability of the halo in ^{19}C can be understood at a microscopical level. Namely, the low-l (s-wave) components are responsible for the halo formation, while the high-l (d-wave) components, which do not contribute to the halo due to the centrifugal barrier, stabilize the halo via pairing correlations [34, 67–69].

Concerning the tensor force effects, the longitudinal momentum distributions, in a manner similar to the cross sections, are slightly weakened when the π-T coupling is deactivated, as illustrated in Fig. 4. These results are consistent with those presented in Table 1. In comparison to the D-RHFB calculation with full PKO3 ($1/2^{+a}$), the deactivation of the π-T coupling ($1/2^{+c}$) leads to an enhancement of the $2s$ component and a reduction of the $3s$ one. As previously discussed in the results of Fig. 3 (b), such alterations do not bring about significant effects on the neutron dispersion. Accordingly, both reaction cross sections and longitudinal momentum distributions are not much affected, either. Therefore, it can be concluded that the tensor force, carried by the π-PV coupling, enhances the continuum contribution but does not influence the halo distribution significantly,.

4. Summary

In summary, we have employed microscopic D-RHFB theory with PKO3 density functional to study the structure of neutron-rich carbon isotopes. We found that the calculated one- and two-neutron separation energies are in good agreement with the measured data. Moreover, the configuration of the ground state (g.s.) of ^{19}C is predicted as $J^\pi = 1/2^+$ by the D-RHFB calculations with PKO3, in which the tensor force and the continuum effects are treated in a natural way. In conjugation with the Glauber model, one of the reaction observables, namely the longitudinal momentum distributions for the g.s. with spin and parity $J^\pi = 1/2^+$, corroborate the measured data and support ^{19}C halo as a dominant s-wave configuration. In this combination, the tight connection between the $1n$ halo and the g.s. configuration of ^{19}C is verified from microscopic structure to reaction observables in a unified way. Furthermore, it is demonstrated

that the continuum states play a dominant role in describing the RCSs and longitudinal momentum distributions, as well as the halo formation, while the effects of the tensor force carried by the π-PV coupling are not as significant as expected.

Consequently, we conclude that the D-RHFB + Glauber approach is an reliable and promising tool for the search for halo candidates, from the microscopic structure to reaction observables. A new receipt with a fully deformed Glauber model is currently in progress.

Acknowledgements

We would like to thank Prof. H. J. Ong for his useful discussions. This work is partly supported by the National Natural Science Foundation of China under Grant Nos. 12175010 and 12275111, the Strategic Priority Research Program of Chinese Academy of Sciences under Grant No. XDB34000000, the Fundamental Research Funds for the Central Universities lzujbky-2023-stlt01, and the Supercomputing Center of Lanzhou University.

References

[1] Y. Xiao, S.-Z. Xu, R.-Y. Zheng, X.-X. Sun, L.-S. Geng, S.-S. Zhang, One-proton emission from $^{148-151}$Lu in the DRHBc plus WKB approach, Phys. Lett. B 845 (2023).

[2] N. Imai, H. J. Ong, N. Aoi, H. Sakurai, K. Demichi, H. Kawasaki, H. Baba, Z. Dombrádi, Z. Elekes, N. Fukuda, Z. Fülöp, A. Gelberg, T. Gomi, H. Hasegawa, K. Ishikawa, H. Iwasaki, E. Kaneko, S. Kanno, T. Kishida, Y. Kondo, T. Kubo, K. Kurita, S. Michimasa, T. Minemura, M. Miura, T. Motobayashi, T. Nakamura, M. Notani, T. K. Onishi, A. Saito, S. Shimoura, T. Sugimoto, M. K. Suzuki, E. Takeshita, S. Takeuchi, M. Tamaki, K. Yamada, K. Yoneda, H. Watanabe, M. Ishihara, Anomalously Hindered $E2$ strength $B(e2; 2_1^+ \rightarrow 0^+)$ in ^{16}C, Phys. Rev. Lett. 92 (2004) 062501.

[3] H. J. Ong, N. Imai, D. Suzuki, H. Iwasaki, H. Sakurai, T. K. Onishi, M. K. Suzuki, S. Ota, S. Takeuchi, T. Nakao, Y. Togano, Y. Kondo, N. Aoi, H. Baba, S. Bishop, Y. Ichikawa, M. Ishihara, T. Kubo, K. Kurita, T. Motobayashi, T. Nakamura, T. Okumura, Y. Yanagisawa, Lifetime measurements of first excited states in ^{16,18}C, Phys. Rev. C 78 (2008) 014308.

[4] M. Wiedeking, P. Fallon, A. O. Macchiavelli, J. Gibelin, M. S. Basunia, R. M. Clark, M. Cromaz, M.-A. Deleplanque, S. Gros, H. B. Jeppesen, P. T. Lake, I.-Y. Lee, L. G. Moretto, J. Pavan, L. Phair, E. Rodriguez-Vietiez, L. A. Bernstein, D. L. Bleuel, J. T. Harke, S. R. Lesher, B. F. Lyles, N. D. Scielzo, Lifetime Measurement of the First Excited 2^+ State in ^{16}C, Phys. Rev. Lett. 100 (2008) 152501.

[5] M. Petri, P. Fallon, A. O. Macchiavelli, S. Paschalis, K. Starosta, T. Baugher, D. Bazin, L. Cartegni, R. M. Clark, H. L. Crawford, M. Cromaz, A. Dewald, A. Gade, G. F. Grinyer, S. Gros, M. Hackstein, H. B. Jeppesen, I. Y. Lee, S. McDaniel, D. Miller, M. M. Rajabali, A. Ratkiewicz, W. Rother, P. Voss, K. A. Walsh, D. Weisshaar, M. Wiedeking, B. A. Brown, Lifetime Measurement of the 2_1^+ State in ^{20}C, Phys. Rev. Lett. 107 (2011) 102501.

[6] P. Voss, T. Baugher, D. Bazin, R. M. Clark, H. L. Crawford, A. Dewald, P. Fallon, A. Gade, G. F. Grinyer, H. Iwasaki, A. O. Macchiavelli, S. McDaniel, D. Miller, M. Petri, A. Ratkiewicz, W. Rother, K. Starosta, K. A. Walsh, D. Weisshaar, C. Forssén, R. Roth, P. Navrátil, Excited–state transition–rate measurements in ^{18}C, Phys. Rev. C 86 (2012) 011303.

[7] Y. Togano, T. Nakamura, Y. Kondo, J. Tostevin, A. Saito, J. Gibelin, N. Orr, N. Achouri, T. Aumann, H. Baba, F. Delaunay, P. Doornenbal, N. Fukuda, J. W. Hwang, N. Inabe, T. Isobe, D. Kameda, D. Kanno, S. Kim, N. Kobayashi, T. Kobayashi, T. Kubo, S. Leblond, J. Lee, F. M. Marqués, R. Minakata, T. Motobayashi, D. Murai, T. Murakami, K. Muto, T. Nakashima, N. Nakatsuka, A. Navin, S. Nishi, S. Ogoshi, H. Otsu, H. Sato, Y. Satou, Y. Shimizu, H. Suzuki, K. Takahashi, H. Takeda, S. Takeuchi, R. Tanaka, A. G. Tuff, M. Vandebrouck, K. Yoneda, Interaction cross section study of the two–neutron halo nucleus ^{22}C, Phys. Lett. B 761 (2016) 412–418.

[8] T. Baumann, M. Borge, H. Geissel, H. Lenske, K. Markenroth, W. Schwab, M. Smedberg, T. Aumann, L. Axelsson, U. Bergmann, D. Cortina-Gil, L. Fraile, M. Hellström, M. Ivanov, N. Iwasa, R. Janik, B. Jonson, G. Münzenberg, F. Nickel, T. Nilsson, A. Ozawa, A. Richter, K. Riisager, C. Scheidenberger, G. Schrieder, H. Simon, B. Sitar, P. Strmen, K. Sümmerer, T. Suzuki, M. Winkler, H. Wollnik, M. Zhukov, Longitudinal momentum distributions of ^{16,18}C fragments after one–neutron removal from ^{17,19}C, Phys. Lett. B 439 (1998) 256–261.

[9] V. Maddalena, T. Aumann, D. Bazin, B. A. Brown, J. A. Caggiano, B. Davids, T. Glasmacher, P. G. Hansen, R. W. Ibbotson, A. Navin, B. V. Pritychenko, H. Scheit, B. M. Sherrill, M. Steiner, J. A. Tostevin, J. Yurkon, Single-neutron knockout reactions: Application to the spectroscopy of ^{16,17,19}C, Phys. Rev. C 63 (2001) 024613.

[10] N. Kobayashi, T. Nakamura, J. A. Tostevin, Y. Kondo, N. Aoi, H. Baba, S. Deguchi, J. Gibelin, M. Ishihara, Y. Kawada, T. Kubo, T. Motobayashi, T. Ohnishi, N. A. Orr, H. Otsu, H. Sakurai, Y. Satou, E. C. Simpson, T. Sumikama, H. Takeda, M. Takechi, S. Takeuchi, K. N. Tanaka, N. Tanaka, Y. Togano, K. Yoneda, One– and two–neutron removal reactions from the most neutron–rich carbon isotopes, Phys. Rev. C 86 (2012) 054604.

[11] A. Ozawa, O. Bochkarev, L. Chulkov, D. Cortina, H. Geissel, M. Hellström, M. Ivanov, R. Janik, K. Kimura, T. Kobayashi, A. Korsheninnikov, G. Münzenberg, F. Nickel, Y.Ogawa, A. Ogloblin, M. Pfützner, V. Pribora, H. Simon, B. Sitár, P. Strmen, K. Sümmerer, T. Suzuki, I. Tanihata, M. Winkler, K. Yoshida, Measurements of interaction cross sections for light neutron–rich nuclei at relativistic energies and determination of effective matter radii, Nucl. Phys. A 691 (2001) 599–617.

[12] T. Nakamura, N. Fukuda, T. Kobayashi, N. Aoi, H. Iwasaki, T. Kubo, A. Mengoni, M. Notani, H. Otsu, H. Sakurai, S. Shimoura, T. Teranishi, Y. X. Watanabe, K. Yoneda, M. Ishihara, Coulomb Dissociation of ^{19}C and its Halo Structure, Phys. Rev. Lett. 83 (1999) 1112–1115.

[13] R. Kanungo, W. Horiuchi, G. Hagen, G. R. Jansen, P. Navratil, F. Ameil, J. Atkinson, Y. Ayyad, D. Cortina-Gil, I. Dillmann, et al., Proton Distribution Radii of $^{12-19}$C Illuminate Features of Neutron Halos, Phys. Rev. Lett. 117 (10) (2016) 102501.

[14] D. Bazin, W. Benenson, B. Brown, J. Brown, B. Davids, M. Fauerbach, P. Hansen, P. Mantica, D. Morrissey, C. Powell, et al., Probing the halo structure of ^{19,17,15}C and ^{14}B, Phys. Rev. C 57 (5) (1998) 2156.

[15] D. Ridikas, M. H. Smedberg, J. S. Vaagen, M. V. Zhukov, 19–C: the heaviest one–neutron halo nucleus?, Europhys. Lett. 37 (6) (1997) 385.

[16] R. Kanungo, I. Tanihata, Y. Ogawa, H. Toki, A. Ozawa, Halo structure in ^{19}C: a Glauber model analysis, Nucl. Phys. A 677 (1-4) (2000) 171–186.

[17] X.-X. Sun, J. Zhao, S.-G. Zhou, Study of ground state properties of carbon isotopes with deformed relativistic Hartree–Bogoliubov theory in continuum, Nucl. Phys. A 1003 (2020) 122011.

[18] K. Zhang, S. Yang, J. An, S. Zhang, P. Papakonstantinou, M.-H. Mun, Y. Kim, H. Yan, Missed prediction of the neutron halo in ^{37}Mg, Phys. Lett. B 844 (2023) 138112.

[19] L.-Y. Wang, J.-L. An, K.-Y. Zhang, S.-S. Zhang, Search for one–neutron halo nucleus in ^{15,17,19}C from reaction observables, manuscript submitted for publication (2024).

[20] B. Acharya, D. R. Phillips, ^{19}C in halo EFT: Effective–range parameters from Coulomb dissociation experiments, Nucl. Phys. A 913 (2013) 103–115.

[21] X.-N. Cao, Q. Liu, J.-Y. Guo, Interpretation of halo in ^{19}C with complex momentum representation method, Journal of Physics G: Nuclear and Particle Physics 45 (8) (2018) 085105.

[22] S.-Z. Xu, S.-S. Zhang, X.-Q. Jiang, M. S. Smith, The complex momentum representation approach and its application to low-lying resonances in ^{17}O and ^{29,31}F, Nucl. Sci. Tech 34 (1) (2023).

[23] Y. Geng, J. Li, Y. Ma, B. Hu, Q. Wu, Z. Sun, S. Zhang, F. Xu, Excitation spectra of the heaviest carbon isotopes investigated within the CD-Bonn Gamow shell model, Phys. Rev. C 106 (2) (2022) 024304.

[24] W. H. Long, N. Van Giai, J. Meng, Density–dependent relativistic Hartree–Fock approach, Phys. Lett. B 640 (2006) 150 – 154.

[25] W. H. Long, H. Sagawa, N. Van Giai, J. Meng, Shell structure and ρ–tensor correlations in density dependent relativistic Hartree–Fock theory, Phys. Rev. C 76 (2007) 034314.

[26] W. H. Long, P. Ring, N. V. Giai, J. Meng, Relativistic Hartree-Fock-bogoliubov theory with density dependent meson-nucleon couplings, Phys. Rev. C 81 (2010) 024308.

[27] W. H. Long, H. Sagawa, J. Meng, N. Van Giai, Pseudo-spin symmetry in density-dependent relativistic Hartree-Fock theory, Phys. Lett. B 639 (2006) 242 – 247.

[28] H. Liang, W. H. Long, J. Meng, N. V. Giai, Spin symmetry in dirac negative-energy spectrum in density-dependent relativistic Hartree-Fock theory, Eur. Phys. J. A 44 (2010) 119–124.

[29] J. Geng, J. J. Li, W. H. Long, Y. F. Niu, S. Y. Chang, Pseudospin symmetry restoration and the in-medium balance between nuclear attractive and repulsive interactions, Phys. Rev. C 100 (2019) 051301(R).

[30] W. H. Long, T. Nakatsukasa, H. Sagawa, J. Meng, H. Nakada, Y. Zhang, Non-local mean field effect on nuclei near sub-shell, Phys. Lett. B 680 (2009) 428 – 431.

[31] J. J. Li, W. H. Long, J. M. Margueron, N. Van Giai, Superheavy magic structures in the relativistic Hartree-Fock-bogoliubov approach, Phys. Lett. B 732 (2014) 169 – 173.

[32] J. J. Li, J. Margueron, W. H. Long, N. V. Giai, Magicity of neutron-rich nuclei within relativistic self-consistent approaches, Phys. Lett. B 753 (2016) 97–102.

[33] J. Liu, Y. F. Niu, W. H. Long, New magicity N = 32 and 34 due to strong couplings between dirac inversion partners, Phys. Lett. B. 806 (2020) 135524.

[34] W. H. Long, P. Ring, J. Meng, N. Van Giai, C. A. Bertulani, Nuclear halo structure and pseudospin symmetry, Phys. Rev. C 81 (2010) 031302.

[35] X. L. Lu, B. Y. Sun, W. H. Long, et al., Description of carbon isotopes within Relativistic Hartree–Fock–Bogoliubov theory, Phys. Rev. C 87 (3) (2013) 034311.

[36] J. J. Li, W. H. Long, J. L. Song, Q. Zhao, Pseudospin-orbit splitting and its consequences for the central depression in nuclear density, Phys. Rev. C 93 (2016) 054312.

[37] J. J. Li, W. H. Long, J. Margueron, N. V. Giai, ^{48}si: An atypical nucleus?, Phys. Lett. B 788 (2019) 192.

[38] J. Geng, Y. F. Niu, W. H. Long, Unified mechanism behind the even-parity ground state and neutron halo of ^{11}be, Chin. Phys. C 47 (2023) 044102.

[39] H. Z. Liang, N. Van Giai, J. Meng, Spin-isospin resonances: A self-consistent covariant description, Phys. Rev. Lett. 101 (2008) 122502.

[40] H. Z. Liang, N. Van Giai, J. Meng, Isospin corrections for superallowed fermi β decay in self-consistent relativistic random-phase approximation approaches, Phys. Rev. C 79 (2009) 064316.

[41] H. Z. Liang, P. W. Zhao, J. Meng, Fine structure of charge-exchange spin-dipole excitations in ^{16}o, Phys. Rev. C 85 (2012) 064302.

[42] Z. Niu, Y. Niu, H. Liang, W. Long, T. Nikšić, D. Vretenar, J. Meng, β-decay half-lives of neutron-rich nuclei and matter flow in the r-process, Phys. Lett. B 723 (2013) 172 – 176.

[43] Z. H. Wang, T. Naito, H. Liang, W. H. Long, Self-consistent random-phase approximation based on the relativistic Hartree-Fock theory: Role of ρ-tensor coupling, Phys. Rev. C 101 (2020) 064306.

[44] W. H. Long, H. Sagawa, J. Meng, N. Van Giai, Evolution of nuclear shell structure due to the pion exchange potential, Europhys. Lett. 82 (2008) 12001.

[45] L. J. Wang, J. M. Dong, W. H. Long, Tensor effects on the evolution of the $N = 40$ shell gap from nonrelativistic and relativistic mean-field theory, Phys. Rev. C 87 (2013) 047301.

[46] L. J. Jiang, S. Yang, J. M. Dong, W. H. Long, Self-consistent tensor effects on nuclear matter systems within a relativistic Hartree-Fock approach, Phys. Rev. C 91 (2015) 025802.

[47] L. J. Jiang, S. Yang, B. Y. Sun, W. H. Long, H. Q. Gu, Nuclear tensor interaction in a covariant energy density functional, Phys. Rev. C 91 (2015) 034326.

[48] Z. Wang, Q. Zhao, H. Liang, W. H. Long, Quantitative analysis of tensor effects in the relativistic Hartree-Fock theory, Phys. Rev. C 98 (2018) 034313.

[49] J. Geng, J. Xiang, B. Y. Sun, W. H. Long, Relativistic Hartree–Fock model for axially deformed nuclei, Phys. Rev. C 101 (2020) 064302.

[50] J. Geng, W. H. Long, Relativistic Hartree–Fock–Bogoliubov model for axially deformed nuclei, Phys. Rev. C 105 (2022) 034329.

[51] G. A. Lalazissis, T. Niksic, D. Vretenar, P. Ring, New relativistic mean-field interaction with density-dependent meson-nucleon couplings, Phys. Rev. C 71 (2005) 024312.

[52] S.-G. Zhou, J. Meng, P. Ring, Spherical relativistic Hartree theory in a Woods–Saxon basis, Phys. Rev. C 68 (2003) 034323.

[53] J. F. Berger, M. Girod, D. Gogny, Microscopic analysis of collective dynamics in low energy fission, Nucl. Phys. A 428 (1984) 23–36.

[54] L. J. Wang, B. Y. Sun, J. M. Dong, W. H. Long, Odd–even staggering of the nuclear binding energy described by covariant density functional theory with calculations for spherical nuclei, Phys. Rev. C 87 (2013) 054331.

[55] X. Meng, S. Zhang, L. Guo, L. Geng, L. Cao, Isospin-density-dependent pairing from infinite nuclear matter to finite nuclei, Phys. Rev. C 102 (6) (2020).

[56] M. Wang, W. J. Huang, F. G. Kondev, G. Audi, S. Naimi, The AME2020 atomic mass evaluation (II). Tables, graphs and references, Chin. Phys. C 45 (2021) 030003.

[57] B. Abu-Ibrahim, Y. Ogawa, Y. Suzuki, I. Tanihata, Cross section calculations in Glauber model: I. Core plus one–nucleon case, Computer Physics Communications 151 (3) (2003) 369–386.

[58] R. Glauber, Lectures in theoretical physics, Interscience Publishers, New York, 1959.

[59] S. S. Zhang, S. Y. Zhong, B. Shao, M. S. Smith, Self-consistent description of the halo nature of ^{31}Ne with continuum and pairing correlations, Journal of Physics G: Nuclear and Particle Physics 49 (2) (2022) 025102–.

[60] S. Y. Zhong, S. S. Zhang, X. X. Sun, M. S. Smith, Study of the deformed halo nucleus ^{31}Ne with Glauber model based on microscopic self-consistent structures, Science China Physics, Mechanics & Astronomy 65 (6) (2022) 1–9.

[61] J.-L. An, K.-Y. Zhang, Q. Lu, S.-Y. Zhong, S.-S. Zhang, A unified description of the halo nucleus ^{37}Mg from microscopic structure to reaction observables, Phys. Lett. B 849 (2024) 138422.

[62] D. Suzuki, H. Iwasaki, H. Onga, N. Imai, H. Sakurai, T. Nakao, N. Aoi, H. Baba, S. Bishop, Y. Ichikawa, M. Ishihara, Y. Kondoc, T. Kubo, K. Kurita, T. Motobayashi, T. Nakamura, T. Okumura, T. Onishi, S. Ota, M. Suzuki, S. Takeuchi, Y. Togano, Y. Yanagisawa, Lifetime measurements of excited states in ^{17}C: Possible interplay between collectivity and halo effects, Phys. Lett. B 666 (2008) 222–227.

[63] S.-G. Zhou, J. Meng, P. Ring, E.-G. Zhao, Neutron halo in deformed nuclei, Phys. Rev. C 82 (2010) 011301.

[64] D. Tran, H. Ong, G. Hagen, T. Morris, N. Aoi, T. Suzuki, Y. Kanada-En'yo, L. Geng, S. Terashima, I. Tanihata, T. Nguyen, Y. Ayyad, P. Chan, M. Fukuda, H. Geissel, M. Harakeh, T. Hashimoto, T. Hoang, E. Ideguchi, A. Inoue, G. Jansen, R. Kanungo, T. Kawabata, L. Khiem, W. Lin, K. Matsuta, M. Mihara, S. Momota, D. Nagae, N. Nguyen, D. Nishimura, T. Otsuka, A. Ozawa, P. Ren, H. Sakaguchi, C. Scheidenberger, J. Tanaka, M. Takechi, R. Wada, T. Yamamoto, Evidence for prevalent Z = 6 magic number in neutron–rich carbon isotopes, Nat. Comm. 9 (2018) 1594.

[65] S. Y. Zhong, Search for Deformed Halo in Neutron-Rich Neon Isotopes with Glauber model, Master's thesis, School of Physics, Beihang University (2022).

[66] A. Ozawa, Y. Hashizume, Y. Aoki, K. Tanaka, T. Aiba, N. Aoi, H. Baba, B. Brown, M. Fukuda, K. Inafuku, et al., One-and two-neutron removal reactions from ^{19,20}C with a proton target, Phys. Rev. C 84 (6) (2011) 064315.

[67] J. Meng, P. Ring, Relativistic Hartree-Bogoliubov Description of the Neutron Halo in ^{11}Li, Phys. Rev. Lett. 77 (1996) 3963–3966.

[68] J. Meng, P. Ring, Giant halo at the neutron drip line, Phys. Rev. Lett. 80 (1998) 460–463.

[69] J. Meng, H. Toki, S. G. Zhou, S. Q. Zhang, W. H. Long, L. S. Geng, Relativistic Continuum Hartree-Bogoliubov theory for the ground state properties of exotic nuclei, Prog. Part. Nucl. Phys. 57 (2006) 470–563.